

# Spectral evidence for substrate availability rather than environmental control of methane emissions from a coastal forested wetland

Bhaskar Mitra<sup>a,b,\*</sup>, Kevan Minick<sup>c</sup>, Guofang Miao<sup>d</sup>, Jean-Christophe Domec<sup>e</sup>, Prajaya Prajapati<sup>a</sup>, Steve G. McNulty<sup>f</sup>, Ge Sun<sup>f</sup>, John S. King<sup>c</sup>, Asko Noormets<sup>a</sup>

<sup>a</sup> Department of Ecology and Conservation Biology, Texas A&M University, College Station, TX, United States

<sup>b</sup> Northern Arizona University, School of Informatics, Computing and Cyber Systems, Flagstaff, AZ 86011, United States

<sup>c</sup> Department of Forestry and Environmental Resources, North Carolina State University, Raleigh, NC, United States

<sup>d</sup> School of Geographical Sciences, Fujian Normal University, Fuzhou, Fujian Province, China

<sup>e</sup> Bordeaux Sciences Agro, UMR INRA-ISPA 1391, 33195, Gradignan, France

<sup>f</sup> Eastern Forest Environmental Threat Assessment Center, USDA Forest Service, Raleigh, NC, United States

## ARTICLE INFO

### Keywords:

Cross-scale analysis  
Methane  
Plant transportation  
Wavelet analysis  
Water table depth

## ABSTRACT

Knowledge of the dynamics of methane (CH<sub>4</sub>) fluxes across coastal freshwater forested wetlands, such as those found in the southeastern US remains limited. In the current study, we look at the spectral properties of ecosystem net CH<sub>4</sub> exchange ( $NEE_{CH_4}$ ) time series, and its cospectral behavior with key environmental conditions (temperature ( $T_{s,s}$ ), water table (WTD) and atmospheric pressure ( $P_a$ )) and physiological fluxes (photosynthesis (GPP), transpiration (LE), sap flux ( $J_s$ )) using data from a natural bottomland hardwood swamp in eastern North Carolina.  $NEE_{CH_4}$  fluxes were measured over five years (2012 – 2016) that included both wet and dry years. During the growing season, strong cospectral peaks at diurnal scale were detected between  $CH_4$  efflux and GPP, LE and  $J_s$ . This suggests that the well understood diurnal cycles in the latter processes may affect  $CH_4$  production through substrate availability (GPP) and transport (sap flow and LE). The causality between different time series was established by the magnitude and consistency of phase shifts. The causal effect of  $T_{s,s}$  and  $P_a$  were ruled out because despite cospectral peaks with  $CH_4$ , their phase relationships were inconsistent. The effect of fluctuations in WTD on  $CH_4$  efflux at synoptic scale lacked clear indications of causality, possibly due to time lags and hysteresis. The stronger cospectral peak with ecosystem scale LE rather than  $J_s$  suggested that the evaporative component of LE contributed equally with plant transpiration. Hence, we conclude that while the emission of dissolved gases through plants likely takes place, it may not contribute to higher  $CH_4$  emissions as has been proposed by aerenchymatous gas transport in sedge wetlands. These findings can inform future model development by (i) highlighting the coupling between vegetation processes and  $CH_4$  emissions, and (ii) identifying specific and non-overlapping timescales for different driving factors.

## 1. Introduction

Wetlands sequester nearly 30% of the global soil carbon despite limited geographical range (~ 8%) (Song et al., 2015). Wetlands also contribute significantly to global methane (CH<sub>4</sub>) emissions, a powerful greenhouse gas with a global warming potential 28 times greater than that of carbon dioxide (CO<sub>2</sub>) (IPCC, 2013). A 2.5-fold increase in CH<sub>4</sub> emissions since the preindustrial times has generated increased scrutiny of its contribution from different sources including wetlands, oceans, fossil fuels and rice agriculture (Dlugokencky et al., 2011). Such an

assessment is critical to developing climate mitigation strategies as (i) the coastal wetlands serve as the main defense against hurricanes and sea level rise, which at 3.4 mm yr<sup>-1</sup> is among the fastest in the world (<https://tidesandcurrents.noaa.gov/sltrends/>), and (ii) they represent a significant and unique carbon sink, holding as much as 500 t C ha<sup>-1</sup> in the soil (Johnson and Kern, 2003). The annual CH<sub>4</sub> budget estimates for the world's wetlands range from 92 to 260 Tg yr<sup>-1</sup> (Khalil and Rasmussen, 1983; Walter et al., 2001; Reeburgh, 2003; Denman et al., 2007; Meng et al., 2012) and remains a big uncertainty from the perspective of global CH<sub>4</sub> estimates (Saunois et al., 2016; Melton et al.,

**Abbreviations:** CO<sub>2</sub>, Carbon dioxide; WT, Continuous wavelet transformation; COI, Cone of Influence; CWT, Cross-wavelet transformation; DWT, Discrete wavelet transformation; ET, Evapotranspiration; GPP (umol m<sup>-2</sup> s<sup>-1</sup>), Gross primary productivity; PAR (umol m<sup>-2</sup> s<sup>-1</sup>), Photosynthetically active radiation

\* Corresponding author.

E-mail address: [Bhaskar.Mitra@nau.edu](mailto:Bhaskar.Mitra@nau.edu) (B. Mitra).

<https://doi.org/10.1016/j.agrformet.2020.108062>

Received 2 July 2019; Received in revised form 21 May 2020; Accepted 29 May 2020

0168-1923/ © 2020 Elsevier B.V. All rights reserved.

**List of symbols**

$P_a$ (kPa)	Atmospheric pressure
$T_a$ (°C)	Air temperature
$P_a$ (kPa)	Atmospheric pressure
$p(x_i y_j)$	Conditional probabilities
$LE$ ( $W\ m^{-2}$ )	Ecosystem-scale latent energy
$H(x)$	Entropy of variable $x$
$H(y)$	Entropy of variable $y$
$J(x,y)$	Joint entropy of $x$ and $y$

$p(x_i,y_j)$	Joint probabilities
$CH_4$ ( $\mu\text{mol}\ m^{-2}\ s^{-1}$ )	Methane
$NEE_{CH_4}$ ( $\mu\text{mol}\ m^{-2}\ s^{-1}$ )	Net ecosystem $CH_4$ exchange
$NEE_{CO_2}$ ( $\mu\text{mol}\ m^{-2}\ s^{-1}$ )	Net ecosystem $CO_2$ exchange
$p$	Probability distribution of measured data
$q$	Probability distribution of modeled data
$J_s$ , ( $g\ m^{-2}\ s^{-1}$ )	Sap flow velocity
$T_{s5}$ (°C)	Soil temperature at 5 cm
$WTD$ (cm)	Water table depth

2013; Bastviken et al. 2011). Such uncertainty primarily exists because of the lack of information about  $CH_4$  exchange across different wetland types as well as insufficient understanding of the drivers of  $NEE_{CH_4}$  (Meronigal and Guenther, 2006; Heimann, 2011; Olefeldt et al., 2013). Improved understanding of the underlying processes and the interaction of different drivers are needed to better capture the magnitude and dynamics of ecosystem  $CH_4$  exchange.

$CH_4$  exchange in wetlands is a multidimensional process.  $CH_4$  production occurs primarily in the anaerobic regions of the soil (Meronigal et al., 2004), although production inside plants has also been hypothesized (Covey and Meronigal, 2019). The emission of dissolved  $CH_4$  in soil water to the atmosphere can occur through diffusion or ebullition (Jeffrey et al., 2019), and may be modified by specialized plant anatomical structure, vascular architecture and rooting volume (Bhullar et al., 2013; Bhullar et al., 2014). The outgassing of  $CH_4$ -saturated water may also occur in plant vasculature, along its transport pathway to leaves (Nesbit et al., 2009). While the transport of dissolved gases in xylem sap has been established (Teskey et al., 2008; Aubrey and Teskey 2009), its precise quantification is difficult. The diffusion of  $CH_4$  through the root and stem spongy tissues (aerenchyma) of some especially wetland-adapted species (e.g. sedges) has been hypothesized to result in elevated emissions compared to non-vegetated surfaces, as the off-gassing of  $CH_4$  through the plant allows it to bypass the microbial re-oxygenation in the anaerobic-aerobic interface in the soil (Bubier and Moore, 1994; Joabsson et al., 1999). Although some tree species also have aerenchymatous tissues (e.g. baldcypress, water tupelo and Atlantic white cedar), its role in ecosystem  $CH_4$  emissions is unclear. Finally, vegetation structure and activity may also affect  $CH_4$  production, as plant-derived carbohydrates may serve as substrates for archaeal methanogens in the soil (Whiting and Chanton, 1993; Christensen et al., 2003; Long et al., 2010). As plant carbohydrate status can affect soil  $CO_2$  production (Mitra et al., 2019), presumably through an effect on microbial substrate availability, it could also be an important regulator of archaeal methanogen activity.

Other well-documented physical drivers of  $CH_4$  production include water table depth ( $WTD$ ), atmospheric pressure, and temperature. Water table position operates as an 'on/off' switch for  $CH_4$  production. Water table drawdown aerates deeper soil horizons, altering the balance between methanogenic archaea and methanotrophic bacteria, reducing net  $CH_4$  efflux. Fluctuations in atmospheric pressure have been shown to facilitate  $CH_4$  release from wetlands, as the dissolution of gases in water is in part controlled by pressure (Tokida et al., 2007). Finally, temperature is often seen as the primary driver of biogeochemical fluxes as it controls the available energy (Arrhenius, 1889; Nahlik and Mitsch, 2011; Sachs et al., 2010), and many models include empirical temperature response functions for  $CH_4$  production while water level acts as a simple on/off switch (Olefeldt et al., 2013; Yvon-Durocher et al., 2014; Turetsky, 2014a,b; Vargas et al., 2010; Treat et al., 2018).

Despite the universality of the temperature and water table response of  $CH_4$  efflux, such simple models oversimplify the system and may limit our ability to interpret observed  $CH_4$  flux dynamics. This is due to the fact that instantaneous combinations of water table and soil

temperature overlooks well-known phenomena like time-lags and hystereses (Hatala et al., 2012; Moore and Dalva, 1993; Sachs et al., 2008; Meijde et al. 2011; Wille et al. 2008). An alternative to this rudimentary approach is a scale-dependent analysis of  $NEE_{CH_4}$  (Sturtevant et al., 2016). Given the number of steps to net  $CH_4$  emission (described above), decomposing the  $CH_4$  signals into low and high-frequency bands may shed light onto  $CH_4$  dynamics and its control mechanisms. This methodology has been successfully applied to identify the multi-scale drivers of  $CO_2$  flux across different biomes (Katul et al., 2001; Stoy et al., 2005; Vargas et al., 2010; Mitra et al. 2019).

In the current study, we will analyze the spectral properties of ecosystem net  $CH_4$  exchange time series, and its cospectral behavior with key environmental conditions (temperature and water table) and physiological processes (photosynthesis, respiration and transpiration) using a 5-year record from a natural bottomland hardwood swamp in eastern North Carolina. We hypothesize that the functional dependence of  $CH_4$  exchange on any of these factors would manifest in co-spectral signatures with them. At the very least, spectral analysis will allow partitioning the sources of variability between fast-changing (radiation, vapor pressure deficit, stomatal conductance, photosynthesis), intermediate or synoptic-scale (atmospheric pressure, soil moisture availability, water table depth), and seasonal processes (seasonal changes in radiation, temperature, phenology). The current study focuses on the variation in  $CH_4$  and its drivers at the first two of the three timescales.

## 2. Methods

### 2.1. Study site

The study site (35°47'16.32"N; 75°54'13.74"W) is located in Alligator River National Wildlife Refuge on the Albemarle-Pamlico peninsula in Dare County of eastern North Carolina, USA. The site is registered as US-NC4 in the Ameriflux database. Established in 1984, Alligator River National Wildlife Refuge is characterized by a heterogeneous conglomeration of pocosin wetland types (Allen et al., 2011).

Overstory vegetation across this freshwater forested wetland consist primarily of water tupelo (*Nyssa aquatica*), red maple (*Acer rubrum*), swamp tupelo (*Nyssa biflora*), along with bald cypress (*Taxodium distichum*), sweetgum (*Liquidambar styraciflua*), white cedar (*Chamaecyparis thyoides*) and loblolly pine (*Pinus taeda*). The understory vegetation consists of fetterbush (*Lyonia lucida*), bitter gallberry (*Ilex alba*), red bay (*Persea borbonia*), and sweet bay (*Magnolia virginiana*). The 30-year (1981-2010) mean temperature and precipitation were 16.9°C and 1270 mm yr<sup>-1</sup> (measured at Manteo airport, NC, about 32 km from the study site). Canopy height across the site ranged from 15 to 20 m, with leaf area index peaking at 4.0 ± 0.3 in early July from a minimum of 1.3 ± 0.3 during the non-growing season (Domec et al., 2015). The pH of soil at the surface varied between 4.2 and 4.8 (Minick et al., 2019b). Bulk density of dry soil was 0.08 ± 0.02 g cm<sup>-3</sup> (mean ± SD). The primary soil types are poorly drained Pungo and Belhaven mucks with their corresponding organic carbon content varying between 40 and 100% and 20 and 100%, respectively (Web Soil Survey; Miao et al., 2017). Precipitation is the primary source of

freshwater for this refuge, and astronomical tides are absent due to the unique combination of geomorphic features and lagoon environments (Moorhead and Brinson, 1995). Other features of this site include the presence of micro-topography, the absence of runoff, and low-intensity drainage.

## 2.2. Gas flux measurements

Ecosystem-scale turbulent fluxes of latent energy ( $LE$ ),  $CO_2$  and  $CH_4$  exchange were measured with eddy covariance method (Baldocchi et al., 1988). The instrumentation consisted of 3-D sonic anemometer thermometer (Windmaster, Gill Instruments Limited, Hampshire, UK), an open path  $CH_4$  analyzer (LI-7700, LI-COR, Lincoln, NE, USA), and an enclosed-path  $CO_2$  and  $H_2O$  analyzer (LI-7200, LI-COR). In addition to turbulent fluxes, we also measured  $CO_2$  concentration (LI-820 infrared gas analyzer and a multi-port system) along a 5-level profile ( $\sim 0.02, 0.04, 0.3, 0.6$  and  $1 \times$  canopy height) in the canopy to estimate canopy storage of  $CO_2$ , which was added to the turbulent fluxes of  $CO_2$  to quantify net ecosystem exchange of  $CO_2$  ( $NEE_{CO_2}$ ). Detailed information on calculation of  $CO_2$  concentration across our site has already been well documented (Miao et al., 2017).

Net ecosystem exchange of  $CH_4$  ( $NEE_{CH_4}$ ) quantified the net  $CH_4$  sequestered or lost by the ecosystem. The sampling frequency of the raw data was 10 Hz and was recorded using a LI-7550 auxiliary interface unit (LI-COR, Nebraska, United States). The average canopy height at the site was 20 m, and the height of the turbulent flux measurements was 28.2 m in 2012, and 33m since 2013.

The turbulent fluxes were calculated and corrections applied with Eddypro software (v 6.1.0, LICOR). The different corrections can be briefly summarized as follows: screening for spikes (Vickers and Mahrt, 1997), rotation of sonic anemometer wind vectors (Wilczak et al., 2001), detrending the raw time series (block averaging), correction of the time lags between scalar concentration and rotated vertical wind speed, and corrections for variations in air density (Webb et al., 1980).

$NEE_{CH_4}$  fluxes measured by the LI-7700 open path analyzer were corrected for spectroscopic effects along with the density corrections (Burba et al., 2019). The spectroscopic corrections are required for narrow band laser analyzers to account for the impact of temperature and pressure on the shape of the absorption feature. High (Ibrom et al., 2007) and low pass (Moncrieff et al., 2004) filtering corrections were also applied, and low-quality flux outputs were discarded (Mauder and Foken, 2006). Post-processing of the 30-minute fluxes include filtering the data corresponding to low signal strength ( $<10\%$ ) and integral turbulence characteristics, removal of outliers (Papale et al., 2006) and friction velocity thresholding (Goulden et al., 1996). As the tower is surrounded by homogeneous vegetation, there was no directional variability in  $NEE_{CH_4}$ . Final data coverage of  $NEE_{CH_4}$  and  $NEE_{CO_2}$  were 27-47% and 60-75% respectively, depending on a year.  $NEE_{CO_2}$  (Supp. Figure S1) was partitioned to gross primary productivity ( $GPP$ ) and ecosystem respiration by modeling nighttime  $NEE_{CO_2}$  as a function of air temperature using a  $Q_{10}$  model. This particular function was used to predict day and night ecosystem respiration and  $GPP$  was quantified as the sum of  $NEE_{CO_2}$  and modeled ecosystem respiration.

## 2.3. Meteorological measurements

Micrometeorological variables that were measured above canopy included air temperature ( $T_a$ ) and relative humidity ( $RH$ ; HMP45, Vaisala, Finland), photosynthetically active radiation ( $PAR$ , PARLITE, Kipp & Zonen, Delft, Netherlands (KZ)), precipitation (TE525, Texas Electronics) and atmospheric pressure ( $P_a$ ) was measured using a pressure sensor (CS 105, Campbell Scientific, Logan, UT, USA). Belowground measurements include soil temperature at 5 cm ( $T_{s5}$ ) and 20 cm depth ( $T_{s20}$ ; CS107, Campbell Scientific). Water table depth ( $WTD$ ) was measured with a pressure water level data logger (Infinites,

Port Orange, FL, USA). All the meteorological variables were measured at 10 sec interval and averaged every 30 minutes.

## 2.4. Sap flow measurements

Granier-type sap flux sensors were used to monitor transpiration at the individual tree scale (Granier 1985, 1987). Five trees per each predominant species (pond pine, water tupelo, red maple and bald cypress, accounting for more than 75% of the total tree basal area) were instrumented near the instrument tower. The 20 mm sensors were installed on the north side of each tree (at diameter at breast height  $\sim 1.3$  m) to reduce the effect of radiation on sap flow estimates. The sensors were covered with aluminum foil to protect the sap flux sensors from external perturbations, including precipitation, as well as minimize temperature fluctuations that would arise from factors other than the sap flow.

The temperature difference data from each sap flux sensor was converted to sap velocity ( $J_s$ ,  $g\ m^{-2}\ s^{-1}$ ) (Ward et al., 2017). Final  $J_s$  was the basal-area-weighted sum of  $J_s$  of the three main canopy species listed above, with the underlying assumption that fluctuations in  $J_s$  is proportional to transpiration dynamics (Small and McConnell, 2008). Temperature difference data from each sensor were recorded as half-hourly averages using a CR1000 data logger (Campbell Scientific). Further information on sapflow-derived tree transpiration at this site can be found in Domec et al. (2015).

## 2.5. Spectral analysis

To evaluate the contribution of different environmental and physiological factors with different time constants to the temporal dynamics of  $NEE_{CH_4}$ , we analyzed the wavelet spectra of  $NEE_{CH_4}$  and co-spectra of  $NEE_{CH_4}$  with presumed independent scalar ( $GPP$ ,  $LE$ ,  $J_s$ ,  $T_{s5}$ ,  $WTD$ ,  $P_a$ ) time series in the time-frequency domain.  $LE$  and  $J_s$  were used as the proxies of  $CH_4$  transport in tree sap and  $GPP$  represented the impact of carbon assimilation on  $NEE_{CH_4}$ . Wavelet transformation generated average wavelet spectrum, defined as the average variance (or energy) associated with specific frequencies for the whole data period. The dominant scale was identified by the maximum of wavelet variance (Kumar and Foufoula-Georgiou, 1997).

Wavelet analysis is advantageous on account of localization in both temporal and scale domain, making it robust to deal with non-stationarities in data. Continuous wavelet transformation with the Morlet (Grinsted et al., 2004) function was used to investigate the oscillation of  $NEE_{CH_4}$  in space and time. The mathematical theory behind this time series strategy has been extensively documented (Torrence and Compo, 1998; Grinsted et al., 2004; Stoy et al., 2013) and applied in our previous work on soil respiration (Mitra et al., 2019).

Apart from average wavelet spectrum, co-spectral or Cross-wavelet transformation (CWT) analysis also generated heatmap that provided a qualitative assessment if one time series was related to another via phase diagram. This was accomplished by analyzing regions of high correlation (red colored areas in heat maps) and at specific frequency (sub-daily, daily, synoptic) in the heat map. In the heat maps, the vertical axis indicated the different frequencies while the horizontal axis referred to the time of year. The arrows in the heat map only represent a lag at one certain time and frequency. Direction of arrows in the heat maps provide an understanding of the nature of coupling between  $NEE_{CH_4}$  and causal scalar ( $GPP$ ,  $LE$ ,  $J_s$ ,  $T_{s5}$ ,  $WTD$ , or  $P_a$ ) time series. Arrows in the heat map pointing at right and left would indicate positive and negative correlation between  $NEE_{CH_4}$  and drivers, with no lags.  $NEE_{CH_4}$  lagged the driver when arrows pointed at up-right (positive correlation) and down-left (negative correlation) direction. Arrows pointing at up-left and down-right direction indicate the driver lagging  $NEE_{CH_4}$ .

Causality was inferred only when  $NEE_{CH_4}$  (i.e. effect) was either in sync or lagged behind the drivers (i.e. the cause) (Banfi and

Ferrini, 2012). Another critical aspect identified in the heat map is the cone of influence. Cone of influence is defined as the boundary within which wavelet transformation is not affected by edge effects. Transformations beyond the cone of influence are ignored. Edge effect arises from the lack of sufficient low frequency data at the beginning and end of the data series.

Given the time constant of processes of interest in this study, we constrained the sampling rate for cospectra between 12 hours and 30 days. Data were normalized to have zero mean and unit variance and gaps in the data were padded with zeros. Padding with a constant does not affect co-spectral power (Mitra et al., 2019) unless the gaps are systematically distributed (which was not in our data). We confirmed the absence of spurious spectral peaks by using a null time series of red noise with the same gap structure as the observations, and evaluated the WT and CWT spectra and cospectra, similar to Mitra et al. (2019).

## 2.6. Lag quantification

Instead of the heat maps, we adopted the non-decimated discrete wavelet transformation (DWT) with Haar basis function (Mahrt, 1991; Katul et al., 2001) to quantify lags between  $NEE_{CH_4}$  and  $GPP$ ,  $LE$  and  $J_s$  at different scales (Whitcher et al., 2000). For this, the time series of  $NEE_{CH_4}$ ,  $GPP$ ,  $LE$  and  $J_s$  was first decomposed into multiple scales (d1 – d11). The different scales (d1-d11) can broadly be classified into diurnal (1 hour – 1.33 days/ d1-d6), synoptic (2.67 – 21.33 days/ d7-d10) and phenological (42.67 days/d11) frequencies.  $NEE_{CH_4}$  and  $GPP$ ,  $LE$  and  $J_s$  time series at each scale were lagged by  $\pm 12$  hours. Typically,  $J_s$  lags  $LE$  due to water storage within trees (Maltese et al., 2018). This lag time between  $LE$  and  $J_s$  was determined using the above-mentioned approach and adjusted prior to the calculation of their individual lags against  $NEE_{CH_4}$ . The highest statistically significant ( $p < 0.05$ ) cross-correlation wavelet coefficient along with the corresponding lag hours have been reported. If more than one independent

scalars preceded  $NEE_{CH_4}$ , the variable with the shortest lag time was identified as the controlling factor, following Koebisch et al. (2015).

## 2.7. Information theory analysis

Wavelet multiresolution analysis was combined with information theory metrics (Shannon, 1948) to have a better understanding of the mutual dependency between  $NEE_{CH_4}$  and its drivers across different scales. Multiresolution analysis consisted of wavelet transformation of an original time series to compute low and high pass filters (d1 – d11). The Haar basis function (Mahrt, 1991) was used for wavelet transformation.

The information theory metrics of interest was mutual information content. Mutual information content can be defined as the amount of information that can be gained about variable  $x$  when information about another variable  $y$  is provided. Mutual information content is greater than zero, with higher values indicative of a larger reduction in uncertainty. Mathematically, mutual information content (MI) can be expressed as follows:

$$MI(x, y) = H(x) + H(y) - J(x, y) = \sum_i \cdot \sum_j p(x_i, y_j) \log \left( \frac{p(x_i|y_j)}{p(x_i)} \right) \quad (1)$$

Where  $H(x)$  and  $H(y)$  refers to the entropy of each variable and  $J(x, y)$  is the joint entropy, and  $p(x_i, y_j)$  and  $p(x_i|y_j)$  are the joint and conditional probabilities respectively. In this analysis,  $x$  was the  $NEE_{CH_4}$  time series, and  $y$  was each level of high and low band pass filtered versions of  $NEE_{CH_4}$ ,  $GPP$ ,  $LE$ ,  $J_s$ ,  $T_{s5}$ ,  $Pa$ , and  $WTD$ . This allowed us to quantify the contribution of each time scale to the predictive uncertainty of  $NEE_{CH_4}$  surface exchange.

As the different measurements had different magnitude and units, all-time series were normalized to have zero mean and unit variance. This allowed all datasets to be treated equally, before wavelet and cross

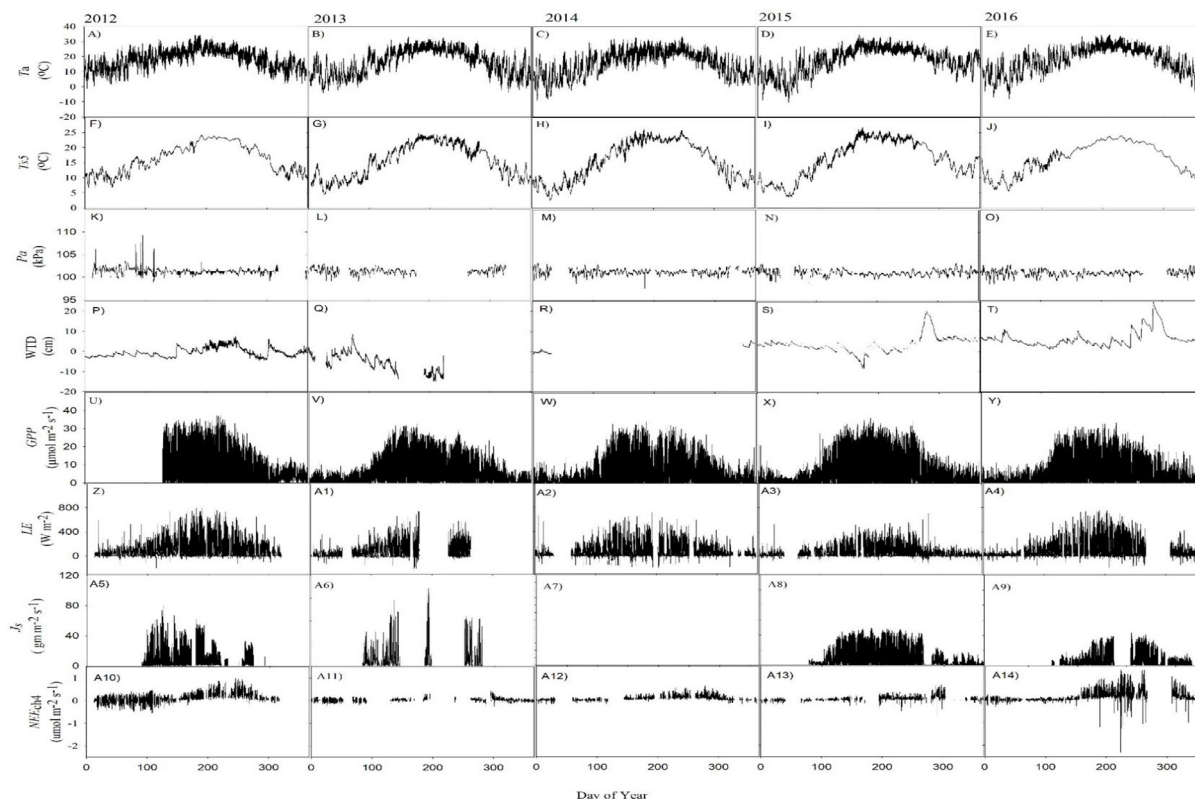


Fig. 1. Seasonal variation of 30-minute air temperature ( $T_a$ ) (Fig. 1A – E), soil temperature at 5 cm depth ( $T_{s5}$ ) (Fig. 1F – J), atmospheric pressure ( $Pa$ ) (Fig. 1K–O), water table depth ( $WTD$ ) (Fig. 1P–T), gross primary productivity ( $GPP$ ) (Fig. 1U–Y), latent energy ( $LE$ ) (Fig. 1Z–A4), sap flux density ( $J_s$ ) (Fig. A5 – A9) and net ecosystem exchange of methane ( $NEE_{CH_4}$ ) (Fig. A10–A14) for US-NC4 across different years (2012, 2013, 2014, 2015, 2016).

analysis. Spectral (“WaveletComp” (Roesch and Schmidbauer, 2014), “waveslim” (Whitcher, 2015)) and information theory (entropy (Hausser and Strimmer, 2009)) analyses were conducted in R (version 3.3.2, R Development Core Team, 2016).

### 3. Results

Daily average air temperature ( $T_a$ ) ranged from 5°C in January to 28°C in July (Fig. 1A-E).  $T_a$  generally remained above 25°C from the middle of June until the end of July. Soil temperature at 5 cm depth ( $T_{s5}$ ) displayed a similar pattern with a lower amplitude (Fig. 1F-J). The most pronounced changes in  $WTD$  were in response to the annual fall storms (Fig. 1P-T). The 5-year study period had normal to above average precipitation compared to the 30-year normal (Supp. Figure S2).  $NEE_{CH4}$  (Fig. 1.A10-A14) had a strong seasonal pattern, increasing from the beginning of May to July, and declining rapidly from September to October, where it stayed near annual minimum until April. Although the seasonality patterns of  $GPP$  (Fig. 1.U-Y),  $LE$  (Fig. 1.Z-A4), and  $J_s$  (Fig. 1.A5-A9) were very similar, their cospectra with  $NEE_{CH4}$  exhibited distinct differences, including distinct differences in the cospectral peak height (Fig. 2).

Oscillation of  $NEE_{CH4}$  was statistically significant at the diurnal scale, with the presence of weak but significant variance also at synoptic scales (Fig. 2A-E). Mutual information between  $CH_4$  and its different band-filtered versions decreased with increase in dyadic time scales (Supp. Fig. S3 A-E). Cospectral analysis between  $NEE_{CH4}$  and  $GPP$  found significant variance at the diurnal scale, and weak but significant interactions at the synoptic scale, as well (Fig. 2F-J). The multiscale analysis found a relative reduction in uncertainty in the estimation of  $NEE_{CH4}$  by  $GPP$  at diurnal time scales (~d3-d6) (Supp. Fig. S3 F-J). The only exception was in 2013 (Fig. S3G) when the lowest reduction in uncertainty was at the phenological time scale (d9-d11).

Heat maps revealed strong correlation between  $GPP$  and  $NEE_{CH4}$  during the growing season (May – September) at the diurnal scale (Period (days) = 1) (Fig. 3A, Supp. Figures S4). The two signals demonstrated a strong covariance with no lags (arrow at right) or  $NEE_{CH4}$  slightly lagged  $GPP$  (arrow at up-right) in 2012 (Fig. 3A), 2014 (Supp. Fig. S4B) and 2016 (Supp. Figure S4D). The relationship between the

two time series was inconsistent in 2013 (Supp. Figure S4A), which we attribute to greater data gaps in this year. Based on direction of arrow in the heat map (down-left or left), there were also brief periods when  $GPP$  and  $NEE_{CH4}$  were negatively correlated (Supp. Fig. S4A & C).

Cospectral analysis between  $NEE_{CH4}$  and  $LE$  (and  $J_s$ ) yielded similar insight with strong variance at daily scale and weak but significant trends at the monthly time step (Fig. 2K-T). Mutual information analysis found the high-frequency band-filtered versions of  $LE$  (scales d4-d6) contributing to a greater reduction of uncertainty of  $NEE_{CH4}$  (Supp. Fig. S3 K-O). Mutual information analysis also found a reduction in the uncertainty for  $NEE_{CH4}$  by  $LE$  at the phenological time scale (d11) (Supp. Figures S3 L-O). Information theory analysis between  $NEE_{CH4}$  and  $J_s$  also yielded similar outcomes (results not shown). The magnitudes of the diurnal cospectral peaks with  $NEE_{CH4}$  were similar, but slightly declining in the order of  $GPP > LE > J_s$  (Fig. 2).

Heat maps highlighted strong correlation between  $NEE_{CH4}$  and  $LE$  at the diurnal scale (Period (days) = 1) (Fig. 3B). Both the fluxes oscillated positively with no lags (arrows pointed at right) in 2012, 2015 and 2016 or  $NEE_{CH4}$  lagged (arrows pointed at up-right)  $LE$  in 2012 (Fig. 3B, Supp. Fig. S5C & D). Data gaps were too large in 2013 (Supp. Fig. S5A) to establish a consistent relationship. In 2014 and 2015, there were instances when  $LE$  fluxes lagged  $NEE_{CH4}$  (arrows at down-right, Supp. Fig. S5B & C).  $LE$  and  $NEE_{CH4}$  were positively coupled at the synoptic scale for brief periods during the growing season in 2012, 2013, and 2014 (Fig. 3B, Supp. Fig. S5A & B). The heat maps between  $NEE_{CH4}$  and  $J_s$  showed similar peaks, but since the peak magnitude was slightly lower (5-35%) than for  $LE$ , the figures are not shown.

$NEE_{CH4} - T_{s5}$  cospectra were characterized by significant interactions at the synoptic scale (Fig. 2U-Y), and with small but statistically significant cycles also detected at the daily time step in 2013, 2014 & 2015 (Fig. 2V-X).  $MI$  analysis found the  $NEE_{CH4} - T_{s5}$  interaction to be also strong at the same time scales in all years (Supp. Fig. S3 P-T). The diurnal timestep of  $T_{s5}$  was also found to significantly reduce uncertainty in  $NEE_{CH4}$  in 2014 and 2015 (Supp. Fig. S3 R & S). Based on direction of arrows in the heat maps, the nature of coupling between  $T_{s5}$  and  $NEE_{CH4}$  was inconsistent at the synoptic scale for all years (Fig. 3C, Supp. Figure S6).

$P_a$  covaried with  $NEE_{CH4}$  at synoptic and monthly frequencies

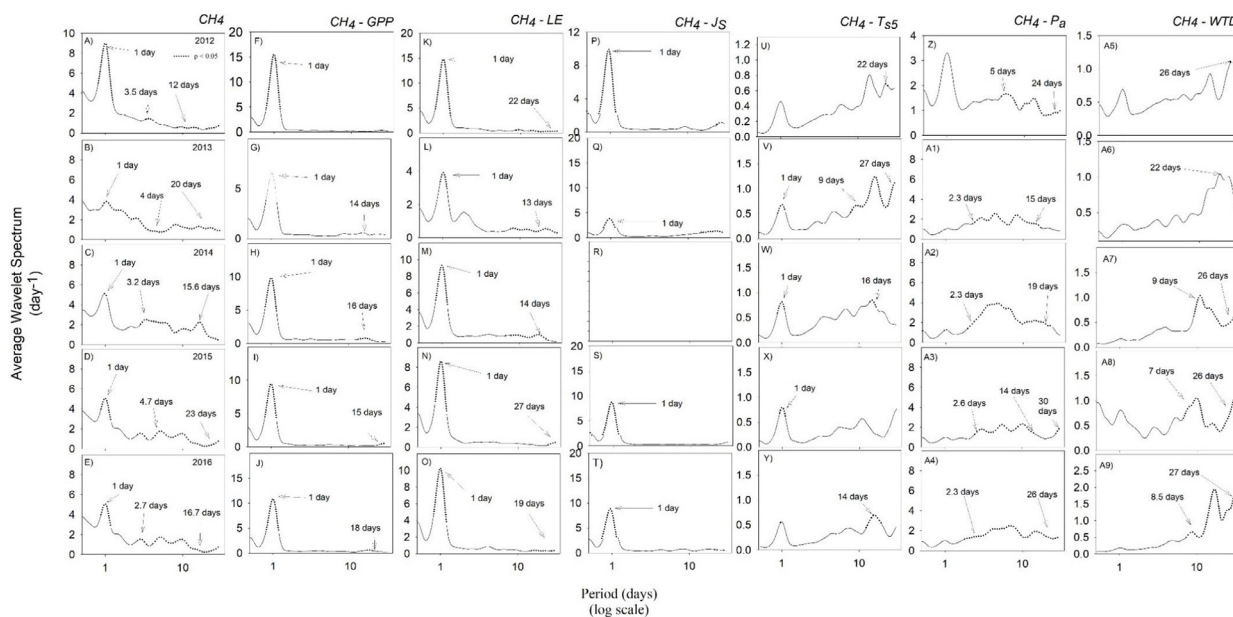
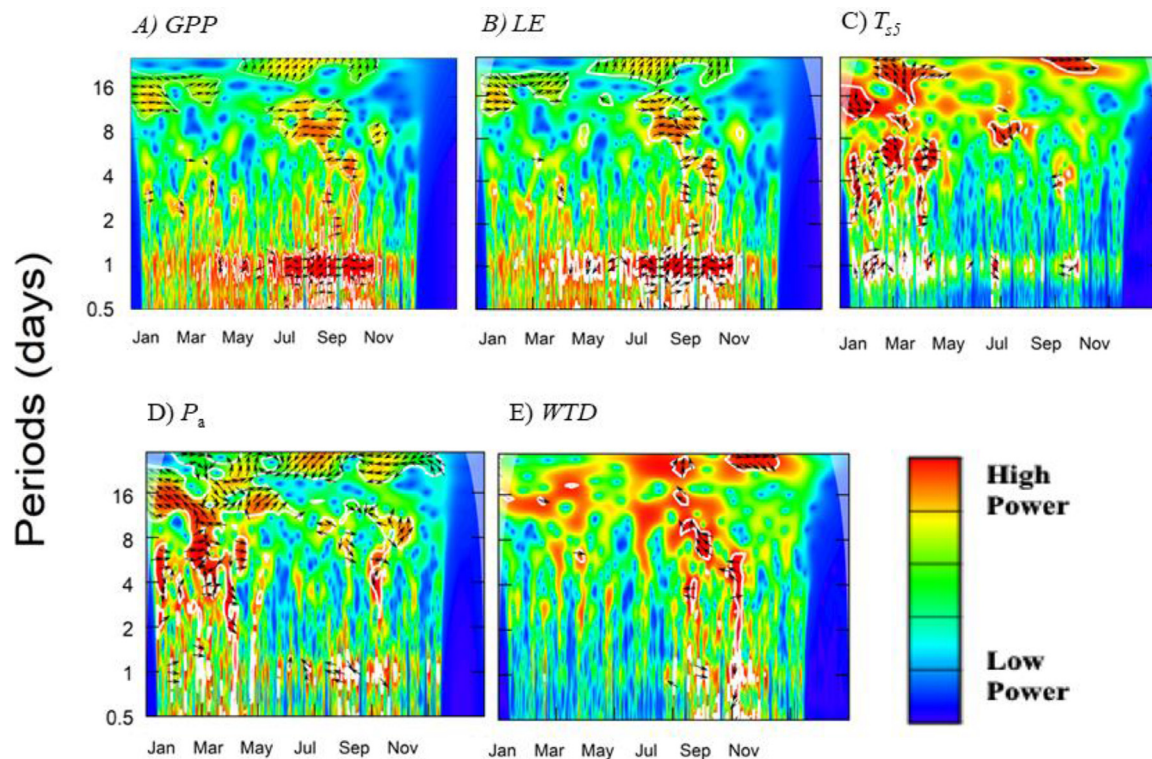


Fig. 2. Average wavelet power in the frequency domain generated across different years for US-NC4 from the wavelet transformation of net ecosystem exchange of methane ( $NEE_{CH4}$ ) (Fig. A-E); continuous wavelet (CWT) transformation between net ecosystem exchange of methane ( $NEE_{CH4}$ ) and gross primary productivity ( $GPP$ ) (Fig. F-J), latent energy ( $LE$ ) (Fig. K-O), sap flux density (Fig. P-T), soil temperature at 5 cm depth ( $T_{s5}$ ) (Fig. U-Y), atmospheric pressure ( $P_a$ ) (Fig. Z-A4) and water table depth ( $WTD$ ) (Fig. A5-A9).



**Fig. 3.** Heat maps highlighting for 2012, the cross-wavelet transformation (CWT) between net ecosystem exchange of methane ( $NEE_{CH_4}$ ) and different drivers including A) gross primary productivity (GPP); B) latent energy (LE); C) soil temperature at 5 cm depth ( $T_{55}$ ); D) atmospheric pressure ( $P_a$ ) and E) water table depth (WTD). Arrows in the heat map pointing at right and left would indicate positive and negative correlation between  $NEE_{CH_4}$  and drivers, with no lags.  $NEE_{CH_4}$  lagged the driver when arrows pointed at up-right (positive correlation) and down-left (negative correlation) direction. Arrows pointing at up-left and down-right direction indicate the driver lagging  $NEE_{CH_4}$ . Red colored areas in heat maps surrounded by white lines indicate areas with 5% significance level.

(Fig. 2Z-A4). This was supported by the multiscale analysis, which found  $MI$  to increase exponentially, highlighting the importance of low-frequency components of  $P_a$  driving the dynamics of  $NEE_{CH_4}$  (Supp. Fig. S3 U-Y). In the heat maps, areas of high common power between  $P_a$  and  $NEE_{CH_4}$  during the early part of the growing season yielded no consistent relationship from periods 4-16 days across all years (Fig. 3D, Supp. Fig. S7).

Cospectral analysis between  $NEE_{CH_4}$  and WTD was characterized by significant interactions at the synoptic and monthly scale (Fig. 2A5-A9).  $MI$  analysis also found the longest time scales of water table dynamics (d12, Supp. Fig. S3 Z-A4) driving the variation in  $NEE_{CH_4}$  exchange. In the heat maps, strong correlation between WTD and  $NEE_{CH_4}$  corresponding to periods greater than four days were primarily concentrated during the late fall season (Supp. Fig. S7C & D). Arrows in the heat maps could not definitely establish casuaslty as  $NEE_{CH_4}$  sometimes lagged (arrows pointed at up-right and down-left) and sometimes lead (arrows pointing at up-left) water table fluctuations.

The degree of association for  $NEE_{CH_4}$  with GPP, LE and  $J_s$  was quantitatively analyzed for dyadic scale 6 (~ 1.3 days) during the growing season as the strongest variance between the time series were concentrated during that particular phase (Fig. 3A&B, Supp. Fig. S4 & S5). GPP and  $NEE_{CH_4}$  were positively correlated with the latter (effect) lagging the former (cause) by 0-4.5 hours at scale 6 (Fig. 4A).  $J_s$  lagged LE by 0.5 to 1.5 hours (2012 – 2016) at dyadic scale 6. After adjusting for this lag time, the lag analysis for  $NEE_{CH_4}$  with LE (&  $J_s$ ) found the latter leading the former only in 2012 and 2013, with shorter lag for LE in 2013 (Fig. 4B & C). The lags were shorter in both years for LE than for GPP.

**4. Discussion**

Scalar analysis of  $CH_4$  variability has both theoretical and practical

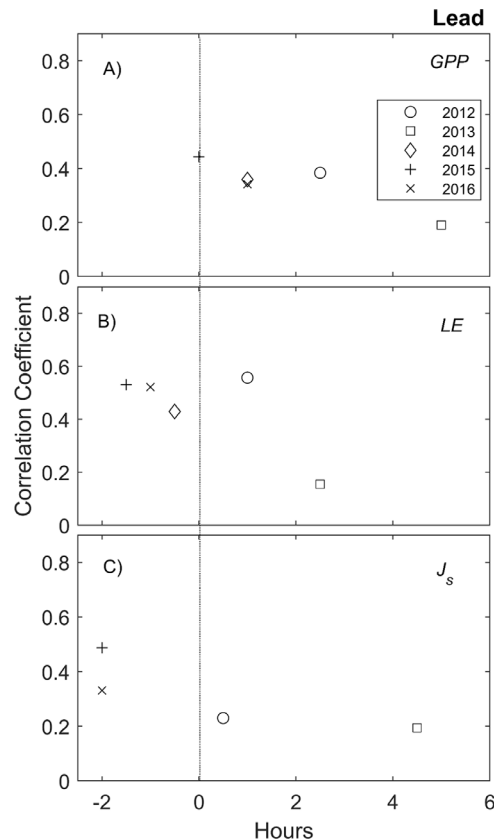


**Fig. 4.** Degree of association (lag/lead) of  $NEE_{CH_4}$  with GPP (A), LE (B), and  $J_s$  (C) for dyadic scale 6 (~ 1.3 days).

implications. By identifying the requisite scale and time, the predictive relationship between CH<sub>4</sub> and biotic/abiotic drivers can be improved with potential to reduce uncertainty in CH<sub>4</sub> budget (Yates et al., 2007). It can also help to develop a comprehensive theoretical framework with regard to the drivers of  $NEE_{CH_4}$ . While the full development of these capabilities is beyond the scope of this study, our results offer strong support to the view that the short-term variability in methane is driven by substrate availability from photosynthesis, while correlations with environmental conditions appear merely coincidental, resulting from the same radiation signal that drives GPP.

$NEE_{CH_4}$  exhibited significant variance at sub-daily and diurnal scale with weak variance at synoptic, and phenological timescales (Fig 2A-E, Supp. Fig. S3A-E). Although the finding of systematic diurnal structure in  $NEE_{CH_4}$  is not universal, it is consistent with the reports of Dacey and Klug (1979), Raimbault et al. (1977), Joabsson et al. (1999), Hatala et al. (2012), Godwin et al. (2013) and Matthes et al. (2014), and follows the spectral properties reported for  $NEE_{CO_2}$  (Katul et al., 2001; Braswell et al., 2005; Stoy et al., 2009; Mitra et al., 2019).

Assuming that the power spectrum of response variables ( $NEE_{CH_4}$  in this case) is influenced by the power spectra of environmental and biological forcing, and that a cause precedes effect, we will attribute the control of  $NEE_{CH_4}$  to different environmental factors and biological processes based on the power cospectra of these different driving variables with  $NEE_{CH_4}$ , and the phase lag between the two time series. For example, the strong cospectral peak between  $NEE_{CH_4}$  and GPP at the daily frequency (Fig. 2F-J, Supp. Fig. S3 F-J) is consistent with earlier observations across a wide range of wetlands, from subarctic peatlands to subtropical marshes (Whiting and Chanton, 1993; Matthes et al., 2014). The consistency in the phase direction (arrow at right or upright) between  $NEE_{CH_4}$  and GPP (Fig. 3A, Supp. Fig. S4), suggest a possible causal connection between the two time series. This hypothesis of  $NEE_{CH_4}$  regulation by carbohydrate substrate supply from GPP is supported by observations that new photosynthates are the preferred carbon substrate for methanogens (Chanton and Whiting, 1996; Minoda and Kimura, 1994; Hatala et al. 2012; Dorodnikov et al., 2011; Ström et al., 2012).

The length of the time lag between GPP and  $NEE_{CH_4}$  (a few hours; Fig. 4A) is consistent with the rate of spread of carbohydrate pressure-concentration waves throughout the plant (Thompson and Holbrook, 2003), and similar to time lags being observed between GPP and soil CO<sub>2</sub> efflux in many earlier reports (Mitra et al., 2019; Liu et al., 2006). It is important to note that studies using tracer analysis invariably observe longer time periods for actual mass flow of carbohydrates (Kuzyakov and Gavrichkova, 2010; Mencuccini and Hölttä, 2010; Wingate et al., 2010). The mass flow of carbohydrates has a finite and rather uniform speed, usually around 20-30 cm hr<sup>-1</sup>, and thus the delay of assimilation and label detection in target tissues is proportional to the length of the transport pathway, whereas pressure-concentration waves alter carbohydrate availability throughout the plant at a shorter timescale, and the effect is independent of distances involved (Kuzyakov and Gavrichkova, 2010; Thompson and Holbrook, 2003).

There were also periods when GPP and the  $NEE_{CH_4}$  time series were either decoupled (Supp. Fig. S4B) or negatively correlated (Supp. Fig. S4A & C). This could be indicative of suppressed CH<sub>4</sub> production and emission (for example, possibly due to increased CH<sub>4</sub> oxidation; Strom et al., 2005; Bouchard et al., 2007), or the dominance of an alternative control mechanism over substrate limitation. One such alternative mechanism could be the transport of dissolved CH<sub>4</sub> with xylem sap, that is then released with transpiration, or that could also diffuse out through the stem along the way (Barba et al., 2019). This would explain the strong covariance of CH<sub>4</sub> at diurnal scale with both LE and  $J_s$  (Fig. 2K-T, Supp. Fig. S3 K-O). Like GPP, LE and  $J_s$  are tightly regulated by stomatal conductance, and partitioning their effect on  $NEE_{CH_4}$  with spectral analysis tools is challenging. The cospectral peak between LE and GPP (Supp. Figure S9, only shown for 2012) is very similar in shape to the cospectrum of  $NEE_{CH_4}$  and GPP, except about 4-

fold greater in amplitude. Nevertheless, the lower power of the  $NEE_{CH_4}$  cospectrum with  $J_s$  than with either GPP or LE (Fig. 2) speaks against the dominance of emissions by transport of dissolved CH<sub>4</sub> in the sap. Indeed, the phase angles of the  $NEE_{CH_4}$  and LE also exhibited decoupling at the same time as those of  $NEE_{CH_4}$  and GPP cospectra (Supp Figs S4A, S4C, S5A, S5C).

Finally, the evidence for GPP-mediated control of  $NEE_{CH_4}$  is bolstered by the lag time analysis. It has been proposed that the variable with the shortest lag interval would be the primary driver (Koebsch et al., 2015). There is more and stronger evidence for the substrate availability-based limitation on  $NEE_{CH_4}$  than for stomatally controlled release of CH<sub>4</sub> with the transpiration stream (although the latter is not insignificant). The fact that in some years  $NEE_{CH_4}$  peaks preceded  $J_s$  (and LE) suggests that their relationship was correlative, or confounded by other processes (Supp Figures S5B & S5C). Furthermore, the shorter lag time for  $NEE_{CH_4}$ -LE relationship compared to  $NEE_{CH_4}$ - $J_s$  in 2013 (Fig. 4 B & C) suggest that the evaporative component of ET was equally important to the transport pathway with transpiration. It appears that wherever the evaporation of water occurs, CH<sub>4</sub> dissolved in the water gets released, and the trees do not appear to represent a preferred low-resistance pathway for CH<sub>4</sub> emission (Barba et al., 2019).

The relationship of  $NEE_{CH_4}$  with environmental drivers  $T_s$ ,  $P_a$  and WTD did not lend strong support to widely accepted view of biophysical regulation of CH<sub>4</sub> production in wetlands. While these factors covaried with  $NEE_{CH_4}$  at diurnal to synoptic time scales, similar to earlier reports (e.g. Tagesson et al., 2012; Hanis et al., 2013; Song et al., 2015; Klapstein et al., 2014; Tokida et al., 2007), the phase direction indicating temporal offsets were either inconsistent ( $P_a$ ,  $T_s$ , WTD) (Supp. Figures S6-S8) or negative at diurnal scale ( $T_s$ ) (Supp. Figure S6C), indicating correlative rather than causal relationship with  $NEE_{CH_4}$ .

Large rain events, especially during the hurricane season in the fall, were usually associated with significant changes in  $NEE_{CH_4}$ , and the cospectra of  $NEE_{CH_4}$  and WTD showed strong peaks in 2013, 2015 and 2016 (Fig. 2 A5 – A9), but the phase angles (Supp. Fig. S8) failed to indicate consistent causality in this pattern. We therefore conclude that the effect of water table must have been mediated by some other process, possibly plant physiological status. Alternatively, the cospectra may have been obscured by time lags and hysteretic responses. For example, the substrate pools and activation times of different microbial populations may cause delayed responses on account of short-lived peaks in water table (e.g. Kettunen et al., 1999; Blodau and Moore, 2003; Knorr et al., 2008). It is also possible that there is a threshold response of  $NEE_{CH_4}$  to fluctuations in the water table, for example, as shown for CO<sub>2</sub> by Miao et al. (2013). Similarly, Brown et al. (2014) showed that maximum methanogen activity occurred at a particular critical water table depth at which the redox potential and substrate availability were at the optimum.

While the evidence for GPP-mediated control of  $NEE_{CH_4}$  appears strong and holds up to different angles of scrutiny, it could be asked if omitting CH<sub>4</sub> storage in the canopy profile could have affected the findings. As CH<sub>4</sub> profile was not measured at the study site, the only option for estimating canopy storage was via the single-point rate of change approach (Hollinger et al., 1994), which in our experience is very unreliable for estimating CO<sub>2</sub> storage in tall canopies, including at the current study site. Nevertheless, the inclusion of this storage estimate did not significantly alter the spectral signature of  $NEE_{CH_4}$ , as well as the cospectra with GPP (data not shown). In addition, the magnitude of the daily cospectral peaks and the lag times remained the similar to those without storage.

In summary, these findings call for re-evaluation of the common correlative patterns as the current way to model CH<sub>4</sub> production in wetlands (e.g. Bridgman et al., 2013; Chu et al., 2014; Turetsky et al., 2014). The spectral analysis reported here has identified certain time (growing season) and frequency (diurnal) patterns that dominate the multidimensional interaction between  $NEE_{CH_4}$  and its biotic and abiotic drivers. We posit that the insights of the significance of GPP-mediated

substrate availability for soil microbial activity (Mitra et al., 2019) have the potential to stimulate emergent ideas for model development. One such approach could be time-varying parameters with specific spectral constraints. Second, the role of dissolved CH<sub>4</sub> transport in the sap may benefit from the detailed representation of plant hydraulic properties, and stem water storage that are being introduced to ecosystem models like CLM and Noah-MP (Li & Matheny, personal communication).

## Acknowledgements

Funding for this AmeriFlux core site was provided by the U.S. Department of Energy's Office of Science, US DOE National Institute of Climatic Change Research (08-SC-NICCR-1072), the USDA Forest Service Eastern Forest Environmental Threat Assessment Center (08-JV-11330147-038, 13-JV-11330110-081), the US DOE Terrestrial Ecosystems Program (11-DE-SC0006700) and the National Science Foundation (NSF-IO5 1754893). Maxwell Wightman and Jonathan Furst maintained the site. We thank Dennis Stewart, Scott Lanier and the staff of Alligator River National Wildlife Refuge for site access and logistical support. Data used for this study can be downloaded from the AmeriFlux database (<https://ameriflux.lbl.gov/data/data-availability/>).

## Supplementary materials

Supplementary material associated with this article can be found, in the online version, at [doi:10.1016/j.agrformet.2020.108062](https://doi.org/10.1016/j.agrformet.2020.108062).

## References

- Arrhenius, S., 1889. Über die Reaktionsgeschwindigkeit bei der Inversion von Rohrzucker durch Säuren. *Zeitschrift für Physikalische Chemie* 4, 226–248.
- Baldocchi, D.D., Hicks, B.B., Meyers, T.P., 1988. Measuring biosphere-atmosphere exchanges of biologically related gases with micrometeorological methods. *Ecology* 69 (5), 1331–1340.
- Barba, J., et al., 2019. Methane emissions from tree stems: a new frontier in the global carbon cycle. *New Phytol.* 222 (1), 18–28. <https://doi.org/10.1111/nph.15582>.
- Banfi, F., Ferrini, G., 2012. Wavelet cross-correlation and phase analysis of a free cantilever subjected to band excitation. *Beilstein J. Nanotechnol.* 3, 294–300.
- Bastviken, D., Tranvik, L.J., Downing, J.A., Crill, P.M., Enrich-Prast, A., 2011. Freshwater methane emissions offset the continental carbon sink. *Science* 331 (6013), 50–50.
- Bhullar, G.S., Edwards, P.J., Venterink, H.O., 2013. Variation in the plant-mediated methane transport and its importance for methane emission from intact wetland peat mesocosms. *J. Plant Ecol.* 6 (4), 298–304.
- Bhullar, G.S., Edwards, P.J., Venterink, H.O., 2014. Influence of different plant species on methane emissions from soil in a restored Swiss Wetland. *PLoS One* 9 (2).
- Blodau, C., Moore, T.R., 2003. Experimental response of peatland carbon dynamics to a water table fluctuation. *Aquat. Sci.* 65 (1), 47–62.
- Bouchard, V., Frey, S.D., Gilbert, J.M., Reed, S.E., 2007. Effects of macrophyte functional group richness on emergent freshwater wetland functions. *Ecology* 88 (11), 2903–2914.
- Braswell, B.H., Sacks, W.J., Linder, E., Schimel, D.S., 2005. Estimating diurnal to annual ecosystem parameters by synthesis of a carbon flux model with eddy covariance net ecosystem exchange observations. *Glob. Change Biol.* 11 (2), 335–355.
- Bridgman, S.D., Cadillo-Quiroz, H., Keller, J.K., Zhuang, Q.L., 2013. Methane emissions from wetlands: biogeochemical, microbial, and modeling perspectives from local to global scales. *Glob. Change Biol.* 19 (5), 1325–1346.
- Bubier, J.L., Moore, T.R., 1994. An ecological perspective on methane emissions from northern wetlands. *Trends Ecol. Evol.* 9 (12), 460–464.
- Burba, G., Anderson, A., Komissarov, A., 2019. Accounting for spectroscopic effects in laser-based open-path eddy covariance flux measurements. *Glob. Change Biol.* 25 (2019), 2189–2202.
- Chanton, J.P., Whiting, G.J., 1996. Methane stable isotopic distributions as indicators of gas transport mechanisms in emergent aquatic plants. *Aquat. Bot.* 54 (2–3), 227–236.
- Christensen, T.R., et al., 2003. Factors controlling large scale variations in methane emissions from wetlands. *Geophys. Res. Lett.* 30 (7).
- Chu, H.S., et al., 2014. Net ecosystem methane and carbon dioxide exchanges in a Lake Erie coastal marsh and a nearby cropland. *J. Geophys. Res.-Biogeosci.* 119 (5), 722–740.
- Covey, K.R., Megonigal, J.P., 2019. Methane production and emissions in trees and forests. *New Phytol.* 222 (1), 35–51. <https://doi.org/10.1111/nph.15624>.
- Dacey, J.W.H., Klug, M.J., 1979. Methane efflux from lake-sediments through water lilies. *Science* 203 (4386), 1253–1255.
- Dlugokencky, E.J., Nisbet, E.G., Fisher, R., Lowry, D., 2011. Global atmospheric methane: budget, changes and dangers. *Philos. Trans. R. Soc. A-Math. Phys. Eng. Sci.* 369 (1943), 2058–2072.
- Domec, J.C., King, J.S., Ward, E., Oishi, A.C., Palmroth, S., Radecki, A., Bell, D.M., Miao, G., Gavazzi, M., Johnson, D.M., McNulty, S.G., Sun, G., Noormets, A., 2015. Conversion of natural forests to managed forest plantations decreases tree resistance to prolonged droughts. *For. Ecol. Manag.* 355, 58–71. <https://doi.org/10.1016/j.foreco.2015.04.012>.
- Dorodnikov, M., Knorr, K.H., Kuzyakov, Y., Wilmking, M., 2011. Plant-mediated CH<sub>4</sub> transport and contribution of photosynthates to methanogenesis at a boreal mire: a C-14 pulse-labeling study. *Biogeosciences* 8 (8), 2365–2375.
- Granier, A., 1985. A new method of sap flow measurement in tree stems. *Ann. Des. Sci. Forest.* 42 (2), 193–200.
- Granier, A., 1987. Evaluation of transpiration in a douglas-fir stand by means of sap flow measurements. *Tree Physiol.* 3 (4), 309–319.
- Goulden, M.L., Munger, J.W., Fan, S.M., Daube, B.C., Wofsy, S.C., 1996. Exchange of carbon dioxide by a deciduous forest: Response to interannual climate variability. *Science* 271, 1576–1578.
- Grinsted, A., Moore, J.C., Jevrejeva, S., 2004. Application of the cross wavelet transform and wavelet coherence to geophysical time series. *Nonlinear Processes Geophys.* 11 (5–6), 561–566.
- Hanis, K.L., Tenuta, M., Amiro, B.D., Papakyriakou, T.N., 2013. Seasonal dynamics of methane emissions from a subarctic fen in the Hudson Bay Lowlands. *Biogeosciences* 10 (7), 4465–4479.
- Hatala, J.A., Detto, M., Baldocchi, D.D., 2012. Gross ecosystem photosynthesis causes a diurnal pattern in methane emission from rice. *Geophys. Res. Lett.* 39.
- Heimann, M., 2011. Atmospheric science enigma of the recent methane budget. *Nature* 476 (7359), 157–158.
- Hollinger, D.Y., Kelliher, F.M., Byers, J.N., Hunt, J.E., McSeveny, T.M., Weir, P.L., 1994. Carbon dioxide exchange between an undisturbed old-growth temperate forest and the atmosphere. *Ecology* 75 (1), 134–150 1994.
- Ibrom, A., Dellwik, E., Flyvbjerg, H., Jensen, N.O., Pilegaard, K., 2007. Strong low-pass filtering effects on water vapour flux measurements with closed-path eddy correlation systems. *Agric. For. Meteorol.* 147 (3–4), 140–156.
- Jeffrey, L.C., Maher, D.T., Johnston, S.G., Kelaher, B.P., Steven, A., Tait, D.R., 2019. Wetland methane emissions dominated by plant-mediated fluxes: Contrasting emissions pathways and seasons within a shallow freshwater subtropical wetland. *Limnol. Oceanogr.* 0 (0). <https://doi.org/10.1002/lno.11158>.
- Joabsson, A., Christensen, T.R., Wallen, B., 1999. Vascular plant controls on methane emissions from northern peatforming wetlands. *Trends Ecol. Evol.* 14 (10), 385–388.
- Katul, G., et al., 2001. Multiscale analysis of vegetation surface fluxes: from seconds to years. *Adv. Water Res.* 24 (9–10), 1119–1132.
- Kettunen, A., et al., 1999. Methane production and oxidation potentials in relation to water table fluctuations in two boreal mires. *Soil Biol. Biochem.* 31 (12), 1741–1749.
- Khalil, M.A.K., Rasmussen, R.A., 1983. Sources, sinks, and seasonal cycles of atmospheric methane. *J. Geophys. Res.-Oceans* 88 (NC9), 5131–5144.
- Klapstein, S.J., et al., 2014. Controls on methane released through ebullition in peatlands affected by permafrost degradation. *J. Geophys. Res.-Biogeosci.* 119 (3), 418–431.
- Knorr, K.H., Oosterwoud, M.R., Blodau, C., 2008. Experimental drought alters rates of soil respiration and methanogenesis but not carbon exchange in soil of a temperate fen. *Soil Biol. Biochem.* 40 (7), 1781–1791.
- Koebisch, F., Jurasinski, G., Koch, M., Hofmann, J., Glatzel, S., 2015. Controls for multi-scale temporal variation in ecosystem methane exchange during the growing season of a permanently inundated fen. *Agric. For. Meteorol.* 204, 94–105.
- Kumar, P., Foufoula-Georgiou, E., 1997. Wavelet analysis for geophysical applications. *Rev. Geophys.* 35 (4), 385–412.
- Kuzyakov, Y., Gavrichkova, O., 2010. REVIEW: time lag between photosynthesis and carbon dioxide efflux from soil: a review of mechanisms and controls. *Glob. Change Biol.* 16 (12), 3386–3406.
- Liu, Q., Edwards, N.T., Post, W.M., Gu, L., Ledford, J., Lenhart, S., 2006. Temperature-independent diel variation in soil respiration observed from a temperate deciduous forest. *Glob. Change Biol.* 12 (11), 2136–2145.
- Long, K.D., Flanagan, L.B., Cai, T., 2010. Diurnal and seasonal variation in methane emissions in a northern Canadian peatland measured by eddy covariance. *Glob. Change Biol.* 16 (9), 2420–2435.
- Mahrt, L., 1991. Eddy asymmetry in the sheared heated boundary-layer. *J. Atmospheric Sci.* 48 (3), 472–492.
- Maltese, A., Awada, H., Capodici, F., Ciruolo, G., La Loggia, G., Rallo, G., 2018. On the use of the Eddy covariance latent heat flux and sap flow transpiration for the validation of a surface energy balance model. *Remote Sens.* 10 (2), 195. 2018. <https://doi.org/10.3390/rs10020195>.
- Matthes, J.H., Sturtevant, C., Verfaillie, J., Knox, S., Baldocchi, D., 2014. Parsing the variability in CH<sub>4</sub> flux at a spatially heterogeneous wetland: Integrating multiple eddy covariance towers with high-resolution flux footprint analysis. *J. Geophys. Res.-Biogeosci.* 119 (7), 1322–1339.
- Mauder, M., Foken, T., 2006. Impact of post-field data processing on eddy covariance flux estimates and energy balance closure. *Meteorol. Z.* 15 (6), 597–609.
- Megonigal, J.P., Hines, M.E., Visscher, P.T., 2004. Anaerobic metabolism: linkages to trace gases and aerobic processes. In: Schlesinger, W.H. (Ed.), *Biogeochemistry*. Elsevier-Pergamon, Oxford, pp. 317–424.
- Meijide, A., et al., 2011. Seasonal trends and environmental controls of methane emissions in a rice paddy field in Northern Italy. *Biogeosciences* 8 (12), 3809–3821.
- Melton, J.R., et al., 2013. Present state of global wetland extent and wetland methane modelling: conclusions from a model inter-comparison project (WETCHIMP). *Biogeosciences* 10 (2), 753–788.
- Mencuccini, M., Holttta, T., 2010. The significance of phloem transport for the speed with which canopy photosynthesis and belowground respiration are linked. *New Phytol.* 185 (1), 189–203.
- Meng, L., et al., 2012. Sensitivity of wetland methane emissions to model assumptions: application and model testing against site observations. *Biogeosciences* 9 (7), 2793–2819.

- Miao, G.F., et al., 2017. Hydrology and microtopography control carbon dynamics in wetlands: implications in partitioning ecosystem respiration in a coastal plain forested wetland. *Agric. For. Meteorol.* 247, 343–355.
- Miao, G.F., et al., 2013. The effect of water table fluctuation on soil respiration in a lower coastal plain forested wetland in the southeastern U.S. *J. Geophys. Res.-Biogeosci.* 118 (4), 1748–1762.
- Minoda, T., Kimura, M., 1994. Contribution of photosynthesized carbon to the methane emitted from paddy fields. *Geophys. Res. Lett.* 21 (18), 2007–2010.
- Minick, K.J., Li, X., Mitra, B., Noormets, A., King, J.S., 2019b. Water table drawdown alters soil and microbial carbon pool size and isotope composition in coastal freshwater forested wetlands. *Front. For. Glob. Change* doi: 0.3389/ffgc.2019.00007.
- Mitra, B., Miao, G., Minick, K., Gavazzi, M., Sun, G., McNulty, S., King, J.S., Noormets, A., 2019. Disentangling the effects of temperature, moisture and substrate availability on soil CO<sub>2</sub> efflux. *JGR-Biogeosci.* <https://doi.org/10.1029/2019JG005148>.
- Moore, T.R., Dalva, M., 1993. The influence of temperature and water-table position on carbon-dioxide and methane emissions from laboratory columns of peatland soils. *J. Soil Sci.* 44 (4), 651–664.
- Moorhead, K.K., Brinson, M.M., 1995. Response of wetlands to rising sea-level in the lower coastal-plain of north-carolina. *Ecol. Appl.* 5 (1), 261–271.
- Nahlik, A.M., Mitsch, W.J., 2011. Methane Emissions from created riverine Wetlands (vol 30, pg 783, 2010). *Wetlands* 31 (2), 449–450.
- Nisbet, R.E.R., et al., 2009. Emission of methane from plants. *Proc. R. Soc. B-Biol. Sci.* 276 (1660), 1347–1354.
- Olefeldt, D., Turetsky, M.R., Crill, P.M., McGuire, A.D., 2013. Environmental and physical controls on northern terrestrial methane emissions across permafrost zones. *Glob. Change Biol.* 19 (2), 589–603.
- Papale, D., et al., 2006. Towards a standardized processing of Net Ecosystem Exchange measured with eddy covariance technique: algorithms and uncertainty estimation. *Biogeosciences* 3 (4), 571–583.
- Raimbault, M., Rinaudo, G., Garcia, J.L., Boureau, M., 1977. A device to study metabolic gases in the rice rhizosphere. *Soil Biol. Biochem.* 9 (3), 193–196.
- Roesch, A., Schmidbauer, R., (2014). *WaveletComp: Computational Wavelet Analysis*.
- Sachs, T., Giebel, M., Boike, J., Kutzbach, L., 2010. Environmental controls on CH<sub>4</sub> emission from polygonal tundra on the microsite scale in the Lena river delta. *Siberia Glob. Change Biol.* 16 (11), 3096–3110.
- Sachs, T., Wille, C., Boike, J., Kutzbach, L., 2008. Environmental controls on ecosystem-scale CH<sub>4</sub> emission from polygonal tundra in the Lena River Delta. *Siberia. J. Geophys. Res.-Biogeosci.* 113.
- Saunois, M., et al., 2016. The global methane budget 2000–2012. *Earth Syst. Sci. Data* 8 (2), 697–751.
- Shannon, C.E., 1948. A mathematical theory of communication. *Bell Syst. Tech. J.* 27 (3), 379–423.
- Small, E.E., McConnell, J.R., 2008. Comparison of soil moisture and meteorological controls on pine and spruce transpiration. *Ecohydrology* 1 (3), 205–214.
- Song, W.M., et al., 2015. Methane emissions from an alpine wetland on the Tibetan Plateau: neglected but vital contribution of the nongrowing season. *J. Geophys. Res.-Biogeosci.* 120 (8), 1475–1490.
- Stoy, P.C., et al., 2013. Evaluating the agreement between measurements and models of net ecosystem exchange at different times and timescales using wavelet coherence: an example using data from the North American Carbon Program Site-Level Interim Synthesis. *Biogeosciences* 10 (11), 6893–6909.
- Stoy, P.C., et al., 2005. Variability in net ecosystem exchange from hourly to inter-annual time scales at adjacent pine and hardwood forests: a wavelet analysis. *Tree Physiol* 25 (7), 887–902.
- Stoy, P.C., et al., 2009. Biosphere-atmosphere exchange of CO<sub>2</sub> in relation to climate: a cross-biome analysis across multiple time scales. *Biogeosciences* 6 (10), 2297–2312.
- Strom, L., Mastepanov, M., Christensen, T.R., 2005. Species-specific effects of vascular plants on carbon turnover and methane emissions from wetlands. *Biogeochemistry* 75 (1), 65–82.
- Strom, L., Tagesson, T., Mastepanov, M., Christensen, T.R., 2012. Presence of *Eriophorum scheuchzeri* enhances substrate availability and methane emission in an Arctic wetland. *Soil Biol. Biochem.* 45, 61–70.
- Sturtevant, C., et al., 2016. Identifying scale-emergent, nonlinear, asynchronous processes of wetland methane exchange. *J. Geophys. Res.-Biogeosci.* 121 (1), 188–204.
- Tagesson, T., et al., 2012. Land-atmosphere exchange of methane from soil thawing to soil freezing in a high-Arctic wet tundra ecosystem. *Glob. Change Biol.* 18 (6), 1928–1940.
- Thompson, M.V., Holbrook, N.M., 2003. Scaling phloem transport: Water potential equilibrium and osmoregulatory flow. *Plant Cell Environ.* 26, 1561–1577.
- Tokida, T., et al., 2007. Falling atmospheric pressure as a trigger for methane ebullition from peatland. *Glob. Biogeochem. Cycles* 21 (2).
- Tokida, T., et al., 2007. Episodic release of methane bubbles from peatland during spring thaw. *Chemosphere* 70 (2), 165–171.
- Torrence, C., Compo, G.P., 1998. A practical guide to wavelet analysis. *Bull. Am. Meteorol. Soc.* 79 (1), 61–78.
- Turetsky, M.R., et al., 2014. A synthesis of methane emissions from 71 northern, temperate, and subtropical wetlands. *Glob. Change Biol.* 20 (7), 2183–2197.
- Turetsky, M.R., et al., 2014. A synthesis of methane emissions from 71 northern, temperate, and subtropical wetlands. *Glob. Change Biol.* 20 (7), 2183–2197.
- Vargas, R., Detto, M., Baldocchi, D.D., Allen, M.F., 2010. Multiscale analysis of temporal variability of soil CO<sub>2</sub> production as influenced by weather and vegetation. *Glob. Change Biol.* 16 (5), 1589–1605.
- Vickers, D., Mahrt, L., 1997. Quality control and flux sampling problems for tower and aircraft data. *J. Atmos. Oceanic Technol.* 14 (3), 512–526.
- Walter, B.P., Heimann, M., Matthews, E., 2001. Modeling modern methane emissions from natural wetlands 1. Model description and results. *J. Geophys. Res.-Atmos.* 106 (D24), 34189–34206.
- Ward, E.J., et al., 2017. TRACC: an open source software for processing sap flux data from thermal dissipation probes. *Trees-Struct. Funct.* 31 (5), 1737–1742.
- Webb, E.K., Pearman, G.I., Leuning, R., 1980. Correction of flux measurements for density effects due to heat and water-vapor transfer. *Q. J. R. Meteorol. Soc.* 106 (447), 85–100.
- Whitcher, B., Gutter, P., Percival, D.B., 2000. Wavelet analysis of covariance with application to atmospheric time series. *J. Geophys. Res.-Atmos.* 105 (D11), 14941–14962.
- Whiting, G.J., Chanton, J.P., 1993. Primary production control of methane emission from wetlands. *Nature* 364 (6440), 794–795.
- Wilczak, J.M., Oncley, S.P., Stage, S.A., 2001. Sonic anemometer tilt correction algorithms. *Boundary Layer Meteorol.* 99 (1), 127–150.
- Wille, C., Kutzbach, L., Sachs, T., Wagner, D., Pfeiffer, E.M., 2008. Methane emission from Siberian arctic polygonal tundra: eddy covariance measurements and modeling. *Glob. Change Biol.* 14 (6), 1395–1408.
- Wingate, L., Ogee, J., Burlett, R., Bosc, A., Devaux, M., Grace, J., Loustau, D., Gessler, A., 2010. Photosynthetic carbon isotope discrimination and its relationship to the carbon isotope signals of stem, soil and ecosystem respiration. *New Phytol.* 188 (2), 576–589.
- Yates, T.T., Si, B.C., Farrell, R.E., Pennock, D.J., 2007. Time, location, and scale dependence of soil nitrous oxide emissions, soil water, and temperature using wavelets, cross-wavelets, and wavelet coherence analysis. *J. Geophys. Res.-Atmos.* 112 (D9).